Opposite-Side SAR Image Processing for Stereo Viewing

J. Kevin Fullerton
Goodyear Aerospace Corporation, Litchfield Park, AZ 85340
Franz Leberl
Vexcel Corporation, Boulder, CO 80301
Robert E. Marque
Goodyear Aerospace Corporation, Litchfield Park, AZ 85340

ABSTRACT: Opposite-side radar image pairs have been considered unsuitable for stereo viewing. Illimunation differences of the two images of an overlapping pair prevented one from fusing a three-dimensional model. This paper reports on a procedure to process the digital data in such a way that opposite-side radar image pairs can be viewed stereoscopically. This permits one to take advantage of a superior intersection geometry for stereoscopic interpretation and parallax measurements.

INTRODUCTION

STEREO VIEWING of overlapping images is a useful tool for improved photointerpretation and allows identification of homologue points for parallax measurements and for feature extraction. The overlapping stereo images are typically taken by a camera.

Side-looking radar sensors differ conceptually in several ways from common photography and other so-called passive imaging systems; a particularly relevant difference is that the imaged ground is actively illuminated by the radar. Therefore, if an overlapping pair of stereo radar images is produced from two different flight or satellite positions, one will have differences in illumination. This has caused the use of stereoscopic viewing to be more difficult than with passive sensor data, or made it even impossible with radar images (LaPrade, 1963; LaPrade, 1970).

Numerous authors have examined the height measurement accuracies that could be achieved by radar images if stereoscopic measurements were feasible. Theoretical error propagation studies by Rosenfield (1968), Gracie *et al.* (1970), Leberl (1972, 1979 a,b), and practical experiments by Derenyi (1975), Graham (1975, 1976, 1979), Koopmans (1974), Leberl (1976, 1978), Derenyi and Stuart (1984), and DBA-Systems (1974) confirm that the so-called "opposite-side" stereo arrangement is geometrically superior to other arrangements, such as with "same-side" (Table 1). The highest accuracy reported to date is the 7-m RMS height errors (Schanda *et al.*, 1985) employing same-side radar with 2-m ground resolution.

Unfortunately, however, the superior opposite-side geometry cannot be used because image pairs cannot be viewed in stereo if the terrain is not flat: the illumination differences are too pronounced for a viewer to merge the homologue features (Figure 1). Successful stereo viewing usually is, however, feasible with same-side or similar configurations.

Recent technological advances have led from film to digital Synthetic-Aperture Radar (SAR) data in which the radar image is a digital matrix of pixel brightness values. The question is, therefore, whether one can digitally alter the opposite-side radar images in such a manner that a previously "unviewable" data set can be successfully merged into a three-dimensional visual impression. Results from early experiments with film images combining a positive image with a negative one on a three-stage comparator encourage this approach (Yoritomo, 1972).

We will show that such processing indeed is feasible, and we will present some examples. The study reports on stereo viewing, but will also compare some aspects of the accuracy of various stereo radar arrangements. The paper describes digital image processing steps needed to achieve successful stereo viewing, and it demonstrates results based on a set of overlapping image pairs. Actual accuracy evaluations of height measurements are the subject of ongoing work.

GEOMETRIC JUSTIFICATION OF OPPOSITE-SIDE RADAR

General

The geometric comparison of various flight arrangements for stereo radar can be based on simple parallax formulas and error propagation. Such formulas have been presented by various authors and were reviewed by Leberl (1979a). The emphasis of past studies, however, has been on predicting errors in a same-side stereo case. Therefore, the fol-

PHOTOGRAMMETRIC ENGINEERING AND REMOTE SENSING,
Vol. 52, No. 9, September 1986, pp. 1487–1498.

0099-1112/86/5209-1487$02.25/0

TABLE 1. SAME-SIDE VERSUS OPPOSITE-SIDE POSITION ACCURACIES AS PUBLISHED BY VARIOUS AUTHORS

Author	Year	RMS Accuracy (m) Along Track	Across Track	Vertical	Control for 100 km²	Resolution (m)	Radar	Remarks
Gracie	1970	12	8	13	35	17	AN/APQ-102	Opposite-side
Konecny	1972	68	138	240		17	Westinghouse	Opposite-side
		130	428	1548				Same-side
DBA-Systems	1974	27	22	17	1.2	3	AN/ASQ-142	Opposite-side
		30	26	20				Same-side
Derenyi	1975			33		12	Gems 1000	Opposite-side
				177				Same-side

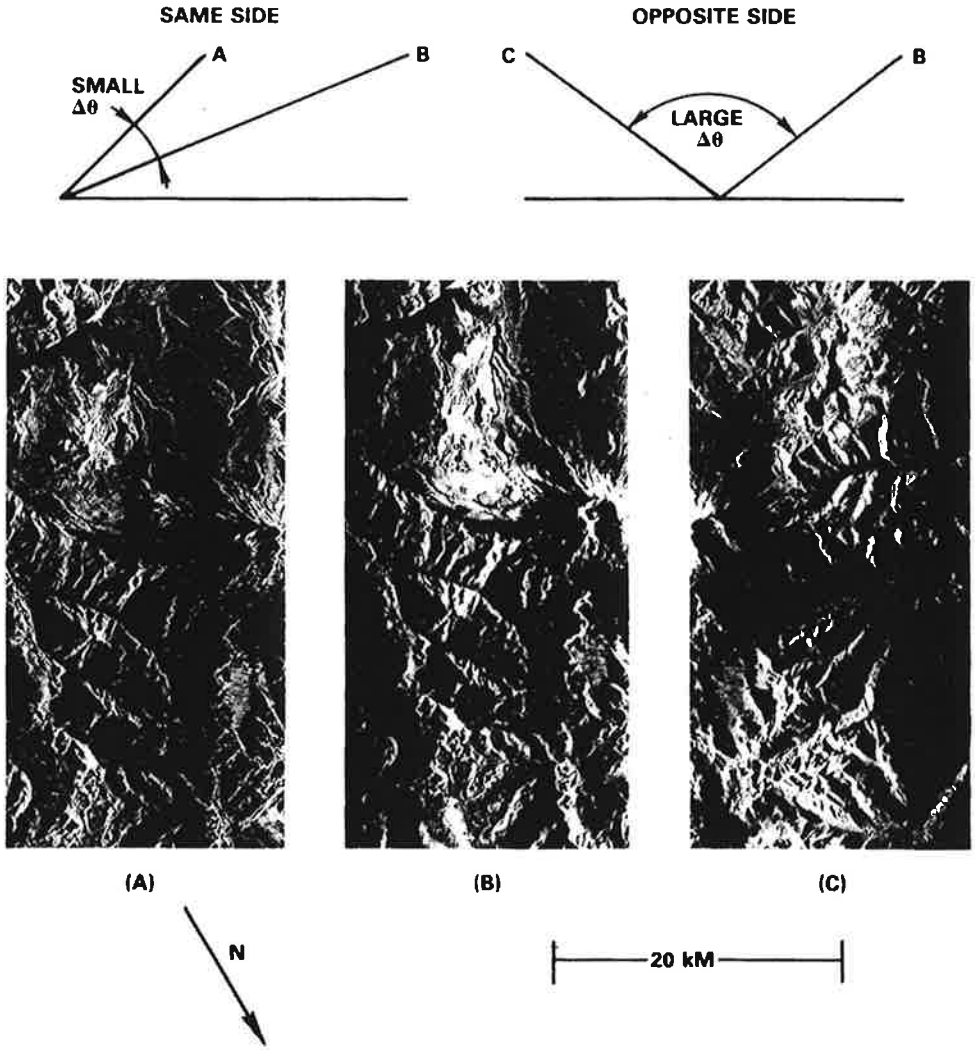

FIG. 1. Examples of same-side (A, B) and opposite-side (B, C) radar stereo image pairs from an area over Mt. St. Helens, Washington. The same-side pair is viewable in stereo while the geometrically superior opposite-side pair cannot be fused. Subsets of this imagery were used throughout.

lowing will specifically address the opposite-side case and relate it to same-side configurations.

Summary of Parallax Equations

Figure 2 defines the entities used to describe radar stereoparallax differences. We find, from Figure 2 for a ground range presentation,

$$dp = pg' + pg'' \tag{1}$$

where

$$pg' = (H - h)\tan\theta' - (1 + h^2/(H^2\sin^2\theta') - 2h/(H\sin^2\theta'))^{1/2}(H\tan\theta')$$

and

$$pg'' = (H - h)\tan\theta'' - (1 + h^2/(H^2\sin^2\theta'') - 2h/(H\sin^2\theta''))^{1/2}(H\tan\theta'').$$

From Figure 2, we find that in the case of slant range presentations a parallax difference exists, even if the terrain were flat. We are only interested in parallax differences, *dps*, due to topographic relief above a reference plane. We therefore define

$$dps = r' + r'' - r'_o - r''_o. \tag{2}$$

In addition, there exists the perceived parallax difference of the datum plane due to the variations of $r'_o - r''_o$ as a function of y; even a flat area will therefore show a systematic bending of the slant range stereo model.

Considering only the relevant parallax difference, dps, we find

$$dps = (H - h)(1/\cos\theta' + 1/\cos\theta'') - H(1/\cos\theta'_o + 1/\cos\theta''_o) \tag{3}$$

where

$$1/\cos\theta'_o = (1 + \tan^2\theta'\,(H - h)^2/H^2)^{1/2} \tag{3a}$$

and

$$1/\cos\theta''_o = (1 + \tan^2\theta''\,(H - h)^2/H^2)^{1/2}. \tag{3b}$$

Figures 3(A) and 3(B) illustrate how Equations 1 and 3 simplify when replacing the spherical radar waves or, geometrically speaking, the circular projection rays by tangents in the object point p: i.e.,

$$dp_g = h\,(\cot\theta' + \cot\theta'') \tag{4}$$

$$dp_s = h\,(\cos\theta' + \cos\theta'') \tag{5}$$

Table 2 presents the size of parallax differences as computed for one terrain height difference of 1 km in four specific configurations shown in Figure 4. The opposite-side cases have larger values dp_s. One should not be misled by the large ground range parallax difference dp_g when one image is at a steep look angle, such as in configuration B. We need to

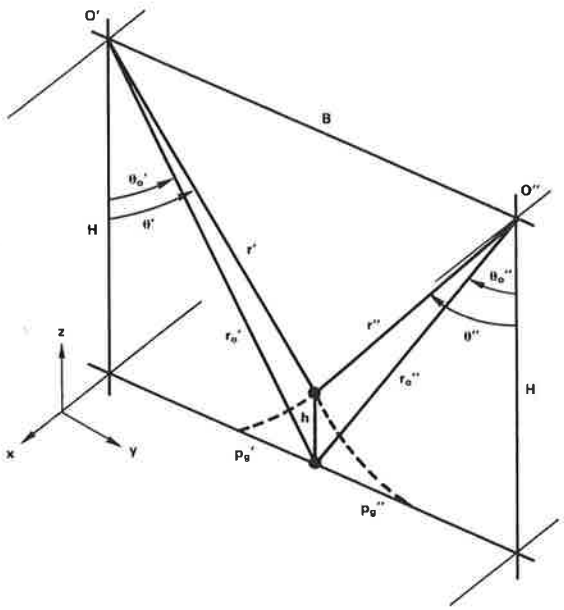

Fig. 2. Entities used for defining radar stereo parallax differences for the ground range and slant range case.

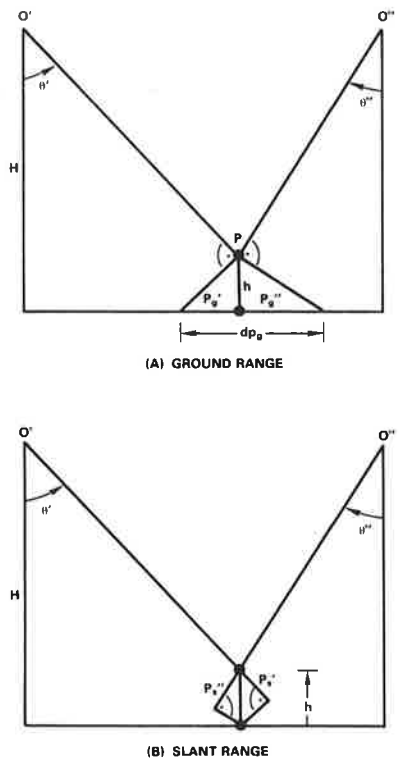

Fig. 3. Simplified radar stereo parallax definitions in ground range and slant range presentations when replacing circular wave fronts by tangent.

TABLE 2. PARALLAX DIFFERENCES COMPUTED FOR VARIOUS RADAR STEREO ARRANGEMENTS, ASSUMING A TERRAIN HEIGHT h = 1 km

Case	Flying Height H (km)	Stereobase B (km)	Look Angles θ′(°)	Look Angles θ″(°)	Look Angles Δθ(°)	Parallax Differences (km) Ground Range	Parallax Differences (km) Slant Range
A	10	11.5	65	45	20	0.53	0.28
B	10	53	80	20	60	2.57	0.77
C	10	34	60	−60	120	1.15	1.00
D	10	20	45	−45	90	2.00	1.40

look at point position errors also in other coordinates than height to be able to compare achievable accuracies.

SUMMARY OF ERROR SENSITIVITY

Error sensitivity formulas were derived in previous work, for example, by Leberl (1979a). Errors discussed there included those of the stereo base, dB, of range, dr, of flying height, dZ, and of the components of the attitude vector. These errors propagate into the computations of point coordinates and of coordinate differences.

Table 3 presents errors arising from the two factors that must be considered major, namely, stereo base error and range resolution. The first, stereo base error, produces coordinate errors and errors of coordinate differences. Coordinate errors (Δy, Δz) are the errors when one attempts to determine the position and height of a point from the stereo pair. Errors of coordinate differences ($d\Delta y$, $d\Delta z$) are applicable when one measures the height differences or distances between points.

Limited range resolution, the second factor, produces standard position and height errors (Δy, Δz). The standard errors are produced by random position errors that vary from point to point. In contrast, the stereo base errors are constant over a large area and their resulting errors of coordinate differences are smaller than the standard errors.

The geometrically superior opposite-side arrangement produces smaller errors than the same-side configuration.

PRELIMINARY CONSIDERATIONS OF STEREO VIEWABILITY

GENERAL

To better understand the effects of radiometric and geometric disparity on stereoscopic viewing, the following questions were raised:

- Is viewability sensitive to brightness/contrast differences?
- What is the importance of low spatial frequencies?
- What is the importance of high frequencies, in particular, edges?
- Is there a mutual reinforcement of geometric and radiometric disparities?

The same-side radar stereo image pairs in Figures 5 and 6 are a basis for the following observations.

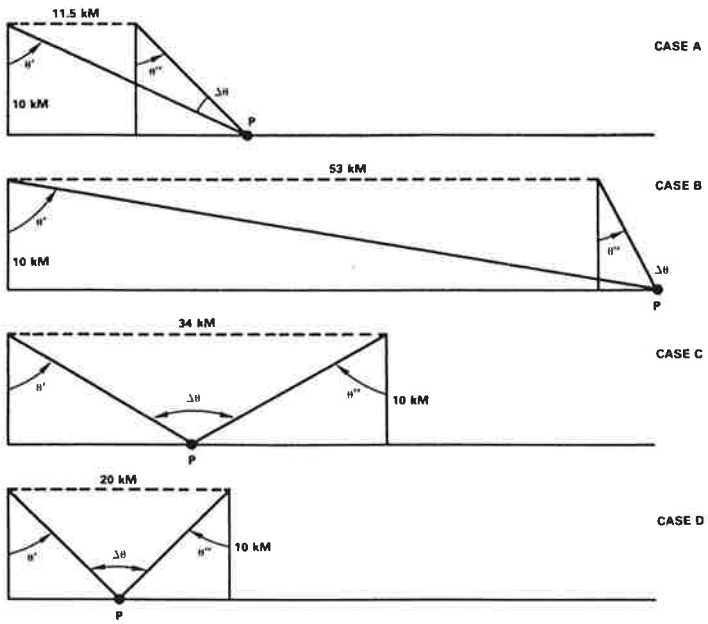

FIG. 4. Four typical radar stereo flight configurations used for error sensitivity computations for Table 2.

TABLE 3. ERRORS OF COORDINATES ($\Delta y, \Delta z$), ERRORS OF COORDINATE DIFFERENCES ($d\Delta y, d\Delta z$), AND STANDARD ERRORS (σ_y, σ_z) ARISING FROM A 100-M STEREO BASE ERROR (dB) AND FROM LIMITED (10-M) RANGE RESOLUTION. ERRORS OF COORDINATE DIFFERENCES, THE ERRORS THAT OCCUR WHEN MEASURING HEIGHT DIFFERENCES, OR THE DISTANCES BETWEEN POINTS, WERE MODELED WITH POINTS SEPARATED BY 1 KM IN RANGE (dy) AND 1KM IN HEIGHT (dy)

Flight Configuration					Errors Due to stereo base error			Range Resolution 10 m			
Case	H (km)	B (km)	θ' (°)	θ'' (°)	$\Delta\theta$ (°)	Δy (m)	$d\Delta y$ (m)	Δz (m)	$d\Delta z$ (m)	σ_y (m)	σ_z (m)
A	10	11.5	65	45	20	−68	−5	−189	−8	9	34
B	10	53	80	20	60	−99	−2	−39	−7	11	12
C	10	34	60	−60	120	50	−3	87	−9	8	14
D	10	20	45	−45	90	50	−5	50	−5	10	10

BRIGHTNESS

The deterioration of the original same-side radar images in Figures 5A, B to 5C, D indicates that the observer can adjust to global brightness differences. The deteriorated pair can be easily viewed in stereo. Similarly, of course, the observer does not get confused if both images of a pair are converted to negatives. If only one is changed to a negative, viewing becomes impossible.

LOW FREQUENCY

A low-pass filtered image pair in Figures 5(E) and (F) still provides an accentuated, viewable stereo pair. However, the lack of higher frequency "stereo clues" does make precise pointing impossible.

HIGH FREQUENCY

The high-pass filtered radar images in Figure 5(G) and (H) cannot be viewed very well under a stereoscope. An edge detector with subsequent edge thinning was used to arrive at the example. Shadow edges contributed to some confusion. Therefore, it becomes clear that all frequencies are needed for stereoscopy.

SEPARATING GEOMETRIC AND RADIOMETRIC DISPARITIES

Figure 6 represents a photographic stereopair with distinctly different illumination but only a small stereo base. Such a case cannot be implemented with radar, but it is necessary to determine whether viewability is possible with large radiometric disparities and small stereo parallaxes. The example of Figure 6 can be viewed in spite of illumination differences. We attribute this fact to the absence of large parallaxes, and to the lack of differences in the high brightness frequencies.

CONCLUSION

One can conclude that all radiometrically similar features are used for stereo viewing. As radiometric differences increase, the visual system seems to be less able to accept stereo parallaxes. The reduction of geometric disparities could compensate for confusion resulting from illumination differences.

As a result, the radar image processing strategy must first make the relative image brightness of common features as similar as possible. Second, geometric processing may be needed to reduce excessive parallax differences if radiometric similarity cannot be achieved to a sufficient degree.

DIGITAL IMAGE PROCESSING OF OPPOSITE-SIDE RADAR STEREO IMAGE PAIRS

GLOBAL POSITIVE-TO-NEGATIVE REMAPPING

Opposite-side illumination effects can be compensated by reversing the brightness of each pixel in one of the two images. This brightness remapping should maintain the average image brightness. Figure 7 presents a typical multilook radar image brightness histogram with its Raleigh power distribution. The remapping function consists of three parts: a center part at a 45-degree slope, a steeper part to remap shadows to the average brightness of slopes facing the antenna, and a flatter part to deal with bright areas that should be made rather dark.

A sloped feature's brightness pattern after positive-to-negative remapping will not precisely match the pattern in the other image of the stereo pair. The brightness patterns will be similar enough to be perceived as the same feature with local small features and textures providing the high spatial frequency clues needed for precise pointing.

Global remapping is only meaningful if the image has a good dynamic range. Should a high-contrast image only contain very bright features on a dark background, then this type of processing is not effective.

Figure 8 illustrates global remapping of the right image of a subset of the Mt St Helens image pair. Note that some features should not have been remapped, such as lakes and a road.

LOCAL BRIGHTNESS REMAPPING

One needs a mechanism to identify image features that should be excluded from global remapping. This could be a set of automated feature extraction methods; in the current experiments this consisted

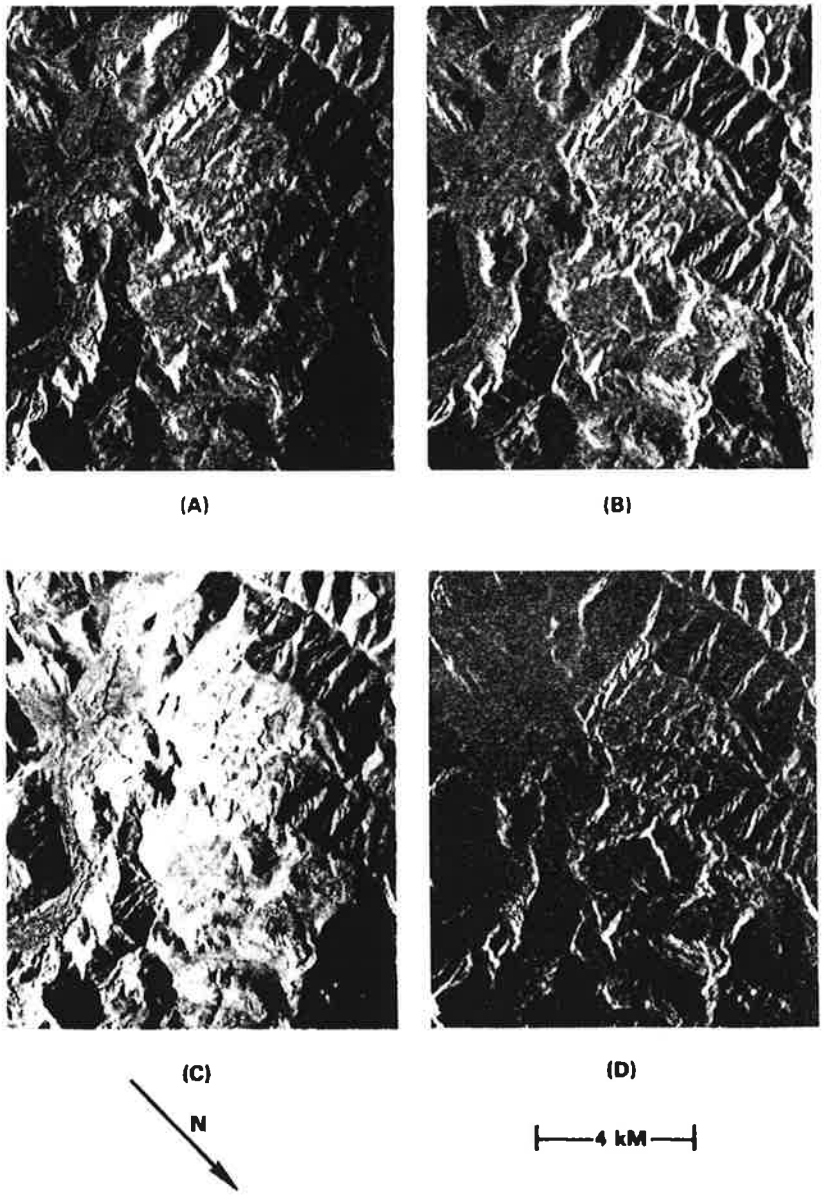

FIG. 5. Same-side radar stereo image subset (A, B) with various processing results. (C) and (D) were remapped with constant pixel brightness shifts, (C) brighter and (D) darker.

of machine-supported manual definition of such features.

Three individual types of local processing must be performed: (a) the undoing of the global remap for certain features, (b) the replacement by random pixel values if confusing features appear in only one image, and (c) individual adjustment of one feature to the brightness it has in the other image.

The process is one of an interactive local "touch-up." The degree to which this step can be fully automated needs to be defined as part of on-going efforts. Figure 9 is the example of Figure 8 after local processing. Most observers can fuse portions of this image pair, but not the entire area.

REDUCING THE PARALLAX DIFFERENCES

Opposite-side radar geometry can produce excessive stereo parallaxes that, combined with brightness differences, confuse the viewer and prevent stereoscopic viewing. Geometric processing reduces the parallax differences with a three-step process.

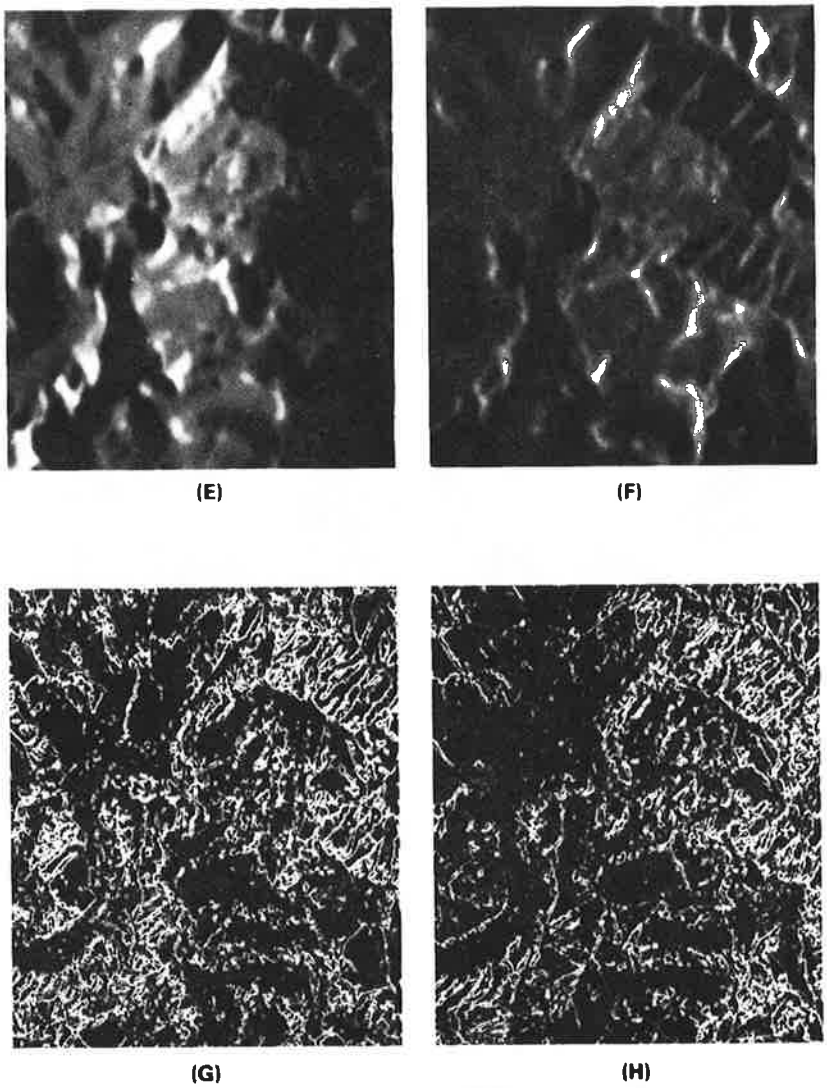

FIG. 5.—Continued. (E) and (F) were low-pass filtered with a 3 by 3 (pixel) uniformly weighted convolution kernel (pixel size is 20 m). (G) and (Y) were first processed with a Robert's edge detector followed by thresholding and edge thinning.

- Preliminary identification of some homologue image points generates widely spaced samples within a sparse topographic relief model
- The sparse model is interpolated to a dense digital elevation model
- The dense model is used to spatially resample one or both of the original images, thereby creating two "near-ortho images."

Opposite-side radar pairs processed to date that contain high to moderate relief require geometric processing to become viewable.

Figure 10 is the final data set after brightness remapping and geometric processing. This reduced parallax pair can be viewed stereoscopically and one can now extract parallax differences that can be converted into terrain height values. These measured height values must be added to the preliminary height values extracted by the geometric processing to obtain the total height measure.

It is not important that the preliminary digital elevation data be accurate. They merely reduce to some extent the geometric disparities in the two images but must be preserved for later use in conjunction with more accurate measurements on the final stereo model.

RESULTS

A series of available opposite-side radar image pairs were processed with the described techniques,

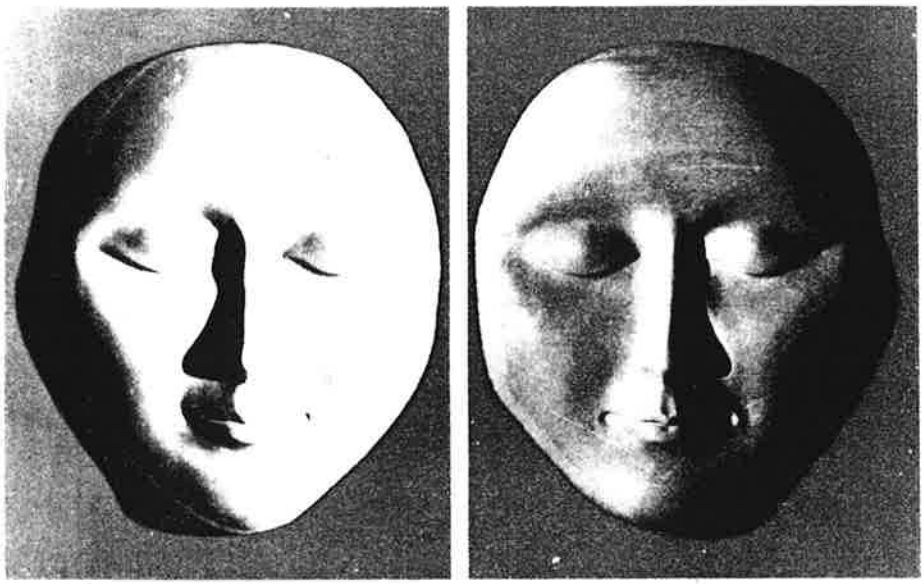

FIG. 6. Stereo photography with small stereo basis and large illumination differences.

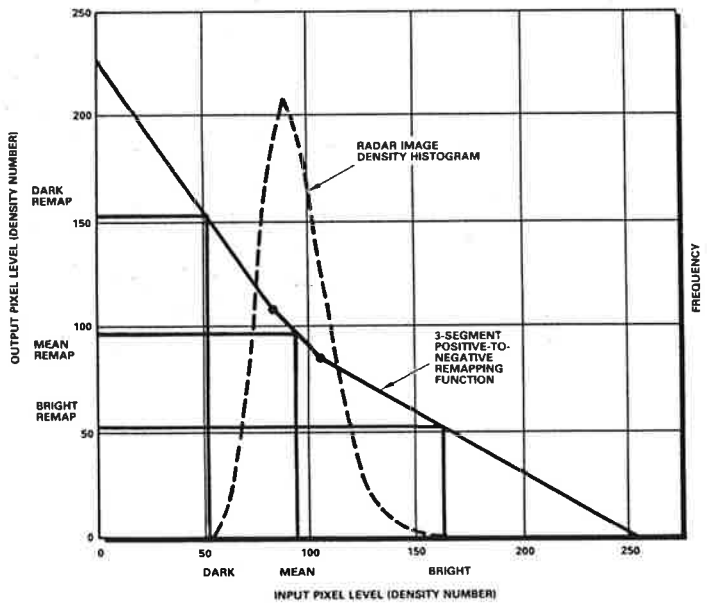

FIG. 7. Radar image brightness histogram and global positive-to-negative remapping function.

employing a digital stereo operator workstation based on two five-inch diagonal flat face, black-and-white monitors horizontally mounted under a mirror stereoscope. The system includes a De Anza IP 8500 image processing system and a VAX 11/780. All image pairs could be viewed successively, with the exception of a part of one image pair around the peak of Mount Saint Helens (Figure 11).

The study did not specifically address the question of height accuracy obtainable from processed opposite-side stereo image pairs; however, one height profile was measured from both the radar data and from a map at a scale of 1:62,500. Only one ground control point was used to determine a datum for the radar-derived heights. The observed radar parallax differences were converted to height using the known values for the look angles θ and θ' in Equation 4. Measurements were repeated to obtain an

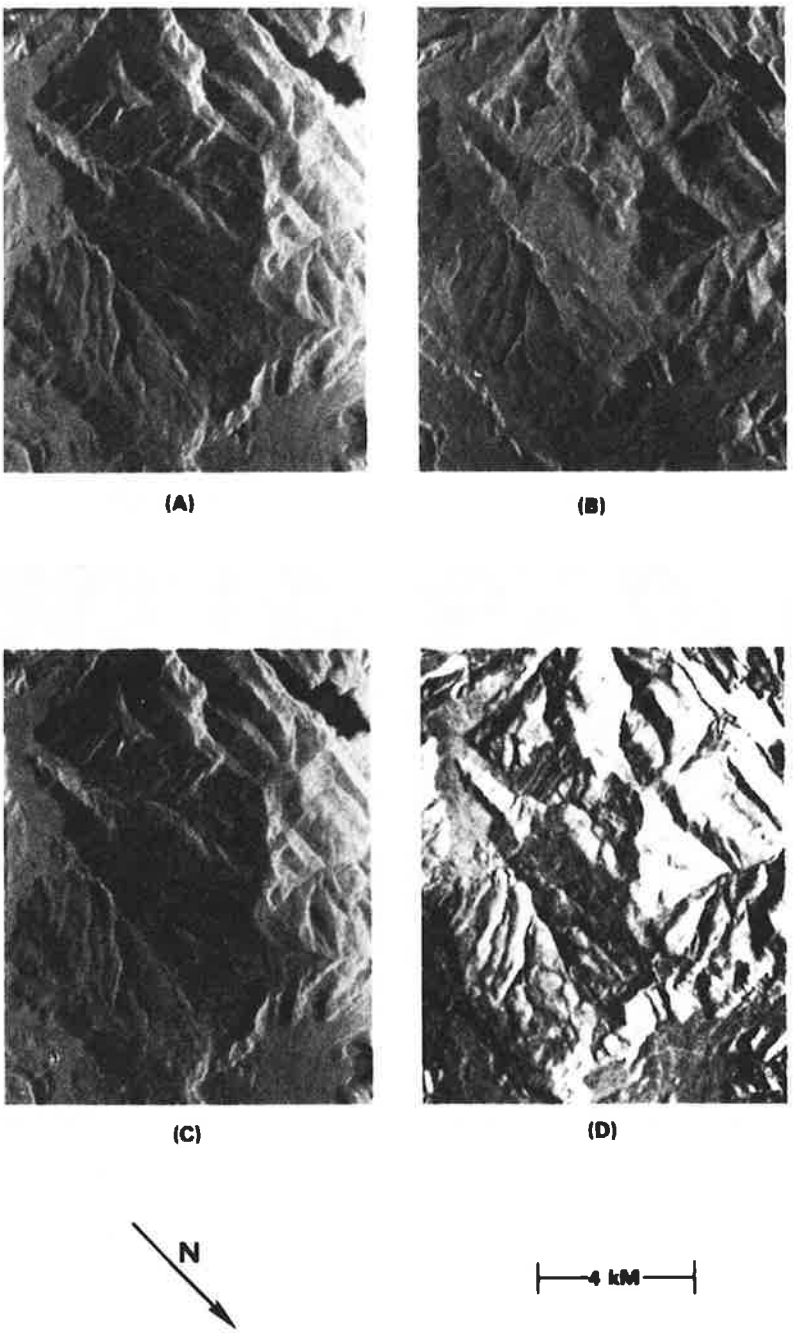

FIG. 8. Subset of Mt. St. Helens opposite-side image stereo pair (A, B). Pair after global remapping of the right image (C, D).

estimate of targeting accuracy. This led to root-mean-square (RMS) errors of ±11 m between repeated pointings.

Measurement difficulties arise when one or both images present a shadow, and when parallel drainage features exist.

Comparison between the radar- and map-derived heights shows an RMS discrepancy of 36 m. This value is obtained with look angles off-nadir of about 45 deg in both images and with a pixel size of 18 m at a near optimum stereo intersection angle of 90

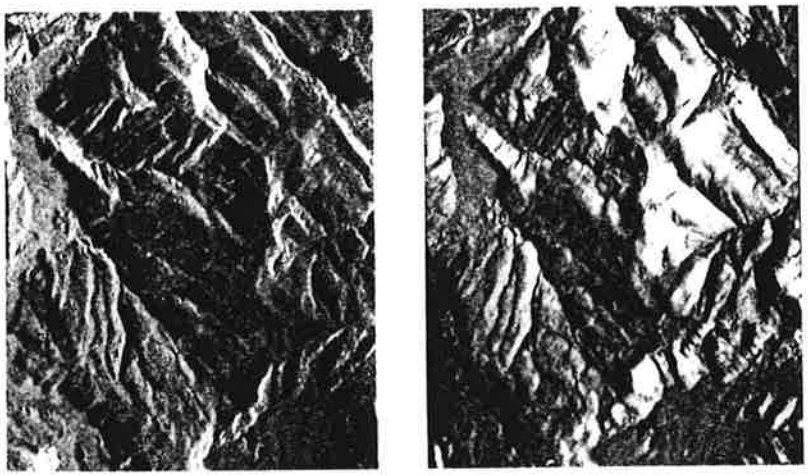

FIG. 9. Result after local remapping of the data from Figure 8.

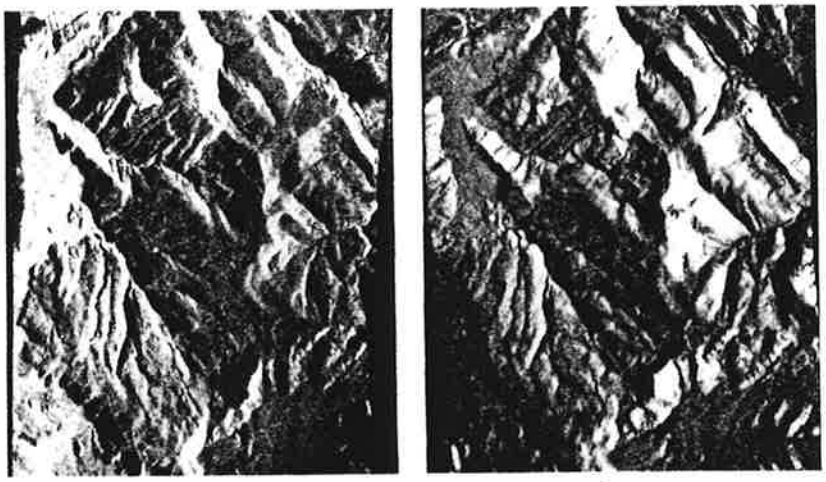

FIG. 10. Result after geometic processing of the data from Figure 9.

deg. The height errors amount, therefore, to about 2 pixels.

One should expect significantly higher accuracies if a rigorous radargrammetric approach is employed with more than one ground control point and with the full resolution potential of the radar system.

CONCLUSIONS AND OUTLOOK

This paper reported on the use of digital image processing techniques to convert opposite-side radar image pairs that were previously unsuitable for stereo viewing to a valid stereoscopically viewable format. The success of the effort is documented by the fact that all of four opposite-side image pairs were modified for good stereoscopy. Only an area around the peak of Mount Saint Helens could not be fused to a three-dimensional model.

Processing consisted of global positive-to-negative remapping of all pixels in one image; subsequent local touch-ups to undo unjustified remapping, *e.g.*, of lakes; and removal of radar features that appear in only one image and confuse the viewer. Finally, the radar images may have to be geometrically resampled to reduce the excessive stereo parallaxes. This results in a coarse, preliminary digital elevation model that can be refined through the final stereoscopic production measurements.

The accuracy potential of the resulting data sets will be investigated in ongoing work. A preliminary set of the height measurements along a profile, taken from a stereo pair at 90-deg intersection angles and at 18-m ground resolution, resulted in RMS errors of 2.0 pixels.

Future work will have to show the accuracy limits with current opposite-side stereo radar imagery where rigorous radargrammetric techniques are used.

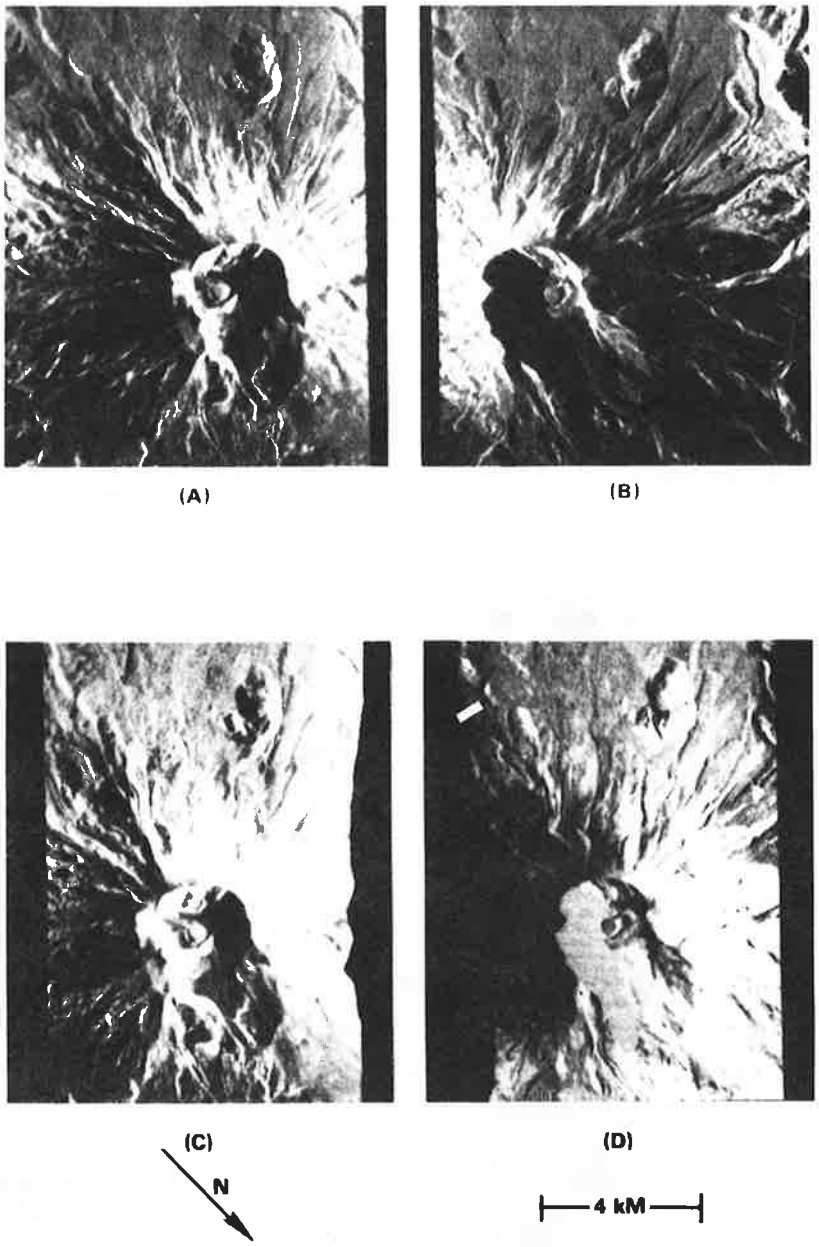

FIG. 11. A second opposite-side stereo image subset with Mt. St. Helens at a 90-degree incidence angle intersection ($\Delta\theta$) before (A, B) and after processing. The peak of Mt. St. Helens cannot be viewed in stereo.

ACKNOWLEDGMENT

Several individuals have greatly supported this effort: Bill Canell and Lee Graham inspired the effort. Lee provided the idea of parallax removal. George LaPrade supported the study with fresh ideas on why one cannot view opposite-side radar images stereoscopically, and how one should modify them. Tim Martin's software turned the VAX/DeAnza combination into an interactive stereo workstation. We are grateful for their support.

The radar stereo imagery was provided by the NASA Johnson Space Center. It was made with an AN/APQ-102A radar modified by Goodyear Aerospace Corporation for the NASA RB-57 platform.

REFERENCES

DBA-Systems, 1974. *Research Studies and Investigations for Radar Control Extensions*, DBA Systems, Inc., P.O. Drawer 550, Melbourne, Florida, Defense Documentation Center Report No. 530784L.

Derenyi, E.E., 1975. Topographical Accuracy of Side-Looking Radar Imagery, *Bildmessung und Luftbildwesen*, Vol. 43, No. 1, pp 68–78.

Derenyi, E., and A. Stuart, 1984. Height Determination from Spaceborne Radar Imagery, *Proceedings ASP Annual Convention*, Washington, DC, pp. 243–252.

Gracie, G., *et al.*, 1970. *Stereo Radar Analysis*, U.S. Engineer Topographic Laboratory, Ft. Belvoir, VA, Report No. FTR-1339-1.

Graham, L., 1975. *Flight Planning for Radar Stereo Mapping*, GERA-2070, Rev A, 21 March 1976, Goodyear Aerospace Corporation, Arizona Division.

———, 1976. *Earth Resources Radar Stereo Considerations*, Goodyear Aerospace Corporation, Arizona Division, AEEM-550, p. 13.

———, 1979. Considerations of Stereo Radar, Workshop on "Radar Geology, an Assessment," Snowmass, Colorado, 16–20 July 1979, JPL Publication 80-61, Pasadena, California.

Konecny, G., 1972. Geometrische Probleme der Fernerkundung, *Bildmessung und Luftbildwesen*, Vol 42, No. 2.

Koopmans, B., 1974. Should Stereo SLAR Imagery be Preferred to Single Strip Imagery for Thematic Mapping?, *ITC Journal* 1974-3, Enschede, The Netherlands.

LaPrade, G.L., 1963. An Analytical and Experimental Study of Stereo for Radar, *Photogrammetric Engineering*, Vol. 29, pp 294–300.

———, 1970. *Subjective Considerations for Stereo Radar*, GIB-9169, Goodyear Aerospace Corporation, Arizona Division.

Leberl, F., 1972. On Model Formation with Remote Sensing Imagery, *Oesterreichische Z. Vermessungswesen*, Vol. 601, No. 2, pp. 43–61.

———, 1976. Imaging Radar Applications to Mapping and Charting, *Photogrammetria*, Vol. 32, No. 3, pp. 75–100.

———, 1978. *Satellitenradargrammetrie*, Deutsche Geodaetische Kommission, Series C, No. 239, Munich, 156 p.

———, 1979a. Accuracy Analysis of Stereo-Side-Looking Radar, *Photogrammetric Engineering and Remote Sensing*, Vol. 45, No. 8, pp. 1083–1096.

———, 1979b. *Accuracy Aspects of Stereo-Side-Looking Radar*, JPL Publication 1979-17, Jet Propulsion Laboratory, Pasadena, USA.

Rosenfield, G.H., 1968. Stereo Radar Techniques, Photogrammmetric Engineering Vol. 34, pp 586–594.

Schanda, E. 1985. A Radargrammetry Experiment in a Mountain Region, *Intl. J. of Remote Sensing*, Vol. 6, No. 7, pp. 1113–1124.

Yoritomo, K., 1972. "Methods and Instruments for the Restitution of Radar Pictures," Invited Paper, 12th Congress of the Intl. Society for Photogrammetry, Ottawa, Canada. In: Arch. Intl. Soc. Photogramm., National Research Council, Ottawa, Canada.

(Received 30 October 1985; accepted 25 February 1986; revised 21 April 1986)
